

Published in final edited form as:

Biofabrication. 2017 March 23; 9(1): 015026. doi:10.1088/1758-5090/aa6265.

Development of a thermosensitive HAMA-containing bio-ink for the fabrication of composite cartilage repair constructs

VHM Mouser^{#1}, A Abbadessa^{#2}, R Levato¹, WE Hennink², T Vermonden², D Gawlitta³, J Malda^{1,4,6}

¹Department of Orthopaedics, University Medical Center Utrecht, PO Box 85500, 3508 GA Utrecht, The Netherlands ²Department of Pharmaceutics, Utrecht Institute for Pharmaceutical Sciences (UIPS), Faculty of Science, Utrecht University, PO Box 80082, 3508 TB Utrecht, The Netherlands ³Department of Oral and Maxillofacial Surgery & Special Dental Care, University Medical Center Utrecht, PO Box 85500, 3508 GA Utrecht, The Netherlands ⁴Department of Equine Sciences, Faculty of Veterinary Medicine, Utrecht University, PO Box 80163, 3508 TD Utrecht, The Netherlands

These authors contributed equally to this work.

Abstract

Fine-tuning of bio-ink composition and material processing parameters is crucial for the development of biomechanically relevant cartilage constructs. This study aims to design and develop cartilage constructs with tunable internal architectures and relevant mechanical properties. More specifically, the potential of methacrylated hyaluronic acid (HAMA) added to thermosensitive hydrogels composed of methacrylated poly[*N*-(2-hydroxypropyl)methacrylamide mono/dilactate] (pHPMA-lac)/polyethylene glycol (PEG) triblock copolymers, to optimize cartilage-like tissue formation by embedded chondrocytes, and enhance printability was explored. Additionally, co-printing with polycaprolactone (PCL) was performed for mechanical reinforcement. Chondrocyte-laden hydrogels composed of pHPMA-lac-PEG and different concentrations of HAMA (0%–1% w/w) were cultured for 28 d *in vitro* and subsequently evaluated for the presence of cartilage-like matrix. Young's moduli were determined for hydrogels with the different HAMA concentrations. Additionally, hydrogel/PCL constructs with different internal architectures were co-printed and analyzed for their mechanical properties. The results of this study demonstrated a dose-dependent effect of HAMA concentration on cartilage matrix synthesis by chondrocytes. Glycosaminoglycan (GAG) and collagen type II content increased with intermediate HAMA concentrations (0.25%–0.5%) compared to HAMA-free controls, while a relatively high HAMA concentration (1%) resulted in increased fibrocartilage formation. Young's moduli of generated hydrogel constructs ranged from 14 to 31 kPa and increased with increasing HAMA concentration. The pHPMA-lac-PEG hydrogels with 0.5% HAMA were found to be optimal for cartilage-like tissue formation. Therefore, this hydrogel system was co-printed with PCL to generate porous or solid constructs with different mesh sizes. Young's moduli of these composite constructs were in the range of native cartilage (3.5–4.6 MPa). Interestingly, the co-

⁶Author to whom any correspondence should be addressed. j.malda@umcutrecht.nl.

printing procedure influenced the mechanical properties of the final constructs. These findings are relevant for future bio-ink development, as they demonstrate the importance of selecting proper HAMA concentrations, as well as appropriate print settings and construct designs for optimal cartilage matrix deposition and final mechanical properties of constructs, respectively.

Keywords

co-printing; thermosensitive hydrogel; PCL reinforcement; methacrylated hyaluronic acid

1 Introduction

Three-dimensional (3D) bioprinting is a promising technique for the fabrication of regenerative constructs. It allows accurate positioning of cells and biomaterials in a layered fashion and can thus be used for the fabrication of organized tissue-like structures [1], e.g. articular cartilage constructs in which a depth-dependent matrix composition and mechanical resistance are addressed [2–4]. Overall, cartilage tissue consists of glycosaminoglycans (GAGs), collagen type II, and water, and contains only a limited number of cells. The low cell number in combination with the lack of vasculature and nerves, leads to the limited regenerative capacity of this tissue [5]. As a consequence, most untreated cartilage defects eventually result in arthritic changes of the whole joint [6]. Therefore, regenerative treatments based on bioprinting to reproduce the cartilaginous organized architecture, are currently under investigation [7–9].

The most commonly used biomaterials for the 3D bioprinting of cartilage constructs are hydrogels, as they allow homogeneous encapsulation of cells and biological cues, and support survival of relevant cell types, i.e. mesenchymal stem cells and chondrocytes. Although hydrogels are potentially suitable for this purpose, optimizing them for bioprinting is challenging. In order to print with high shape-fidelity, the hydrogel needs to possess certain rheological properties, e.g. high yield stress and viscosity, while for cell encapsulation and optimal tissue production by embedded cells, low yield stresses and viscosities are favorable [10, 11]. Hydrogels based on UV-curable copolymers of a polyethylene glycol (PEG) midblock flanked by two partially methacrylated poly[*N*-(2-hydroxypropyl)methacrylamide mono/dilactate] (pHPMA-lac) outer blocks are attractive systems for tissue engineering applications because their characteristics, e.g. *in vitro* degradation rate and mechanical properties can be accurately tuned via adjustments of the building block's architecture and polymer concentration [12–15]. Recently, we have demonstrated that pHPMA-lac-PEG hydrogels with relatively low concentration and degree of methacrylation supported cartilage matrix deposition by embedded chondrocytes [16]. In addition, the partial replacement of pHPMA-lac-PEG triblock copolymers with methacrylated polysaccharides, i.e. hyaluronic acid (HAMA) [16] and chondroitin sulfate [17] further prolonged the *in vitro* degradation profile and enhanced the mechanical properties of the hydrogel blends. Importantly, the addition of HAMA to pHPMA-lac-PEG hydrogels allowed bioprinting with sufficient shape-fidelity of hydrogels even when a relatively low total polymer concentration was used [16]. Hyaluronic acid (HA) and chondroitin sulfate are polysaccharides present in articular cartilage tissue and have been

reported to influence multiple biological processes, e.g. cell proliferation, migration, attachment, and differentiation [18–20]. Especially HA forms an interesting component for cartilage tissue engineering as multiple studies have demonstrated an anabolic effect of both HA and HAMA on chondrocytes in various culture systems *in vitro* and *in vivo* [21–28]. However, several studies also indicated a critical role of the HA or HAMA concentration on chondrogenesis, as too low or too high HA or HAMA concentrations can be ineffective or even inhibitory [25–28]. Therefore, it is important to identify the currently unknown optimal concentration of HAMA in pHPMA-lac-PEG triblocks/HAMA hydrogels for cartilage regeneration.

An additional aspect that has to be taken into account for cartilage repair constructs, is the requirement to withstand the high compressive and shear forces present in the articulating joints. However, the maximum stiffness that any hydrogel can reach, without hampering matrix production of embedded cells, is limited [29]. Multiple reinforcement strategies, such as the inclusion of fibers [30, 31] or microparticles [32], consisting of different materials, e.g. polycaprolactone (PCL) [33–35], poloxamer-based hydrogels [36], and ceramics [37] have been explored. Especially PCL is a promising reinforcement material as it is biocompatible, cost-effective, and it has a relatively slow degradation rate (ranging from months to years) [38]. The co-printing of a (cell-laden) hydrogel with a PCL fiber reinforcement offers a construct design in which the hydrogel provides the necessary milieu for cells to thrive, and the thermoplastic framework provides the required mechanical properties, to overall mimic the biomechanical profile of native cartilage. The mechanical performance of co-printed hydrogel/PCL constructs is dominated by that of the PCL framework [30]. Therefore, by modifying the PCL molecular weight (MW) and the geometry of the PCL skeleton, the compressive modulus and tensile strength can be tailored to that of the target tissue [39]. The strand size, strand distance, and to a lesser extent strand orientation, have been identified as the most important geometrical parameters to influence the mechanical features of the printed construct [33, 39, 40]. Hence, co-printing of pHPMA-lac-PEG triblocks/HAMA hydrogel with PCL might be an attractive approach for the fabrication of cartilage repair constructs. Hence, the aim of this study was to generate bioprinted constructs for cartilage regeneration with optimized bioactivity, and a tunable mechanical performance. As such, the optimal concentration of HAMA in pHPMA-lac-PEG triblocks/HAMA hydrogels for cartilage-like tissue formation of embedded chondrocytes was evaluated, and co-printing with PCL, using multiple construct architectures, was explored to match the mechanical properties of native cartilage.

2 Materials and methods

2.1 Materials

All chemicals were obtained from Sigma-Aldrich (Zwijndrecht, the Netherlands) and all solvents from Biosolve (Valkenswaard, the Netherlands) unless indicated otherwise. Chemicals and solvents were used as received. HA sodium salt (120 kDa) was supplied by Lifecore Biomedical (Chaska, MN, USA) and PEG (10 kDa) by Merck (Darmstadt, Germany). GMP grade homopolymer of ϵ -caprolactone (PCL, Parasorb PC 12, 185001) and L-lactide were obtained from Corbion (Gorinchem, The Netherlands), and Irgacure 2959

was a kind gift of BASF (Ludwigshafen, Germany). *N*-(2-hydroxypropyl) methacrylamide mono- and dilactate, and PEG_{10kDa}-4,4'-azobis(cyanopentanoate) macro-initiator were synthesized as previously reported [41, 42]. Phosphate buffered saline (PBS), penicillin/streptomycin (pen/strep; 10 000 units ml⁻¹ penicillin and 10 mg ml⁻¹ streptomycin) and picogreen DNA assay were supplied by Invitrogen (Carlsbad, California, USA). Fetal bovine serum (FBS) was purchased from Gibco (Invitrogen corporation) and type II collagenase was obtained from Worthington Biochemical Corp (Lakewood, NJ, USA). Two types of Dulbecco's modified eagle medium (DMEM) were used: DMEM 31885 from Gibco (referred to as DMEM) and high glucose DMEM D6429 from Sigma-Aldrich (referred to as high glucose DMEM). Recombinant human TGF-β1 was obtained from Peprotech (London, UK), hyaluronidase (H2126) from Sigma-Aldrich, pronase (11459643001) from Roche Life Sciences (Indiana, USA), and ITS+ premix (human recombinant insulin, human transferrin, selenous acid, bovine serum albumin, linoleic acid) from BD Biosciences (Breda, the Netherlands). Antibody against collagen type I (1:100; EPR7785, ab138492) was obtained from Abcam (Cambridge, UK). Antibodies against collagen types II and VI (1:100; II-6B3II and 1:5, 5C6, respectively) were obtained from the Developmental Studies Hybridoma Bank (Iowa City, IA, USA). Antibody against proteoglycan IV (1:50; H00010216-M01) was obtained from Novus (Abingdon, United Kingdom). Secondary horse radish-peroxidase conjugated antibodies for collagen type I (EnVision+, K4010), collagen type II (1:100, IgG HRP, P0447), collagen type VI and proteoglycan IV (EnVision+, K4007) were ordered from DAKO (Heverlee, the Netherlands). Calcein-AM (to stain living cells) and ethidium homodimer-1 (to stain nuclei of dead cells) were obtained from Life Technologies (L3224, Bleiswijk, the Netherlands).

2.2 Synthesis and characterization of polymers

A triblock copolymer composed of two poly[*N*-(2-hydroxypropyl) methacrylamide mono/dilactate] outer blocks (~15 kDa) flanking a PEG (10 kDa) mid-block, was synthesized and characterized as previously described, and 10% of the hydroxyl groups from the pendent lactate side-unites was methacrylated (chemical structure reported in scheme S1 is available online at stacks.iop.org/BF/9/015026/mmedia) [12]. The methacrylated pHPMA-lac-PEG triblock copolymer is hereafter termed M₁₀P₁₀ [M₁₀ refers to a degree of methacrylation (DM) of 10%, and P₁₀ refers to a PEG block with a MW of 10 kDa]. HA was methacrylated (DM = 10%, indicating the presence of 10 methacrylate groups per 100 disaccharide units) as previously described (chemical structure reported in scheme S1) [43]. The characteristics of M₁₀P₁₀, i.e. number average MW (M_n), polydispersity index (PDI), CP and DM, as well as those of HAMA, i.e. MW and DM were in line with our previous findings [12, 16, 17].

2.3 Experimental design

First, a screening of five different hydrogel formulations (table 1) was performed to find the optimal concentration of HAMA for cartilage tissue engineering with chondrocyte-laden M₁₀P₁₀/HAMA hydrogels. Equine chondrocytes were encapsulated in the different hydrogel formulations and constructs were cast for *in vitro* culture. At days 1 and 28, the hydrogels were harvested and evaluated for cartilage-like tissue formation. In addition, Young's moduli were evaluated for cell-free cast hydrogel constructs of different compositions (table 1).

Second, 3D printed constructs were fabricated with the best performing formulation of the first screening, i.e. MHA_{0.5}. Additionally, multiple constructs with different architectures were fabricated by co-printing MHA_{0.5} and PCL, and the Young's moduli were determined.

2.4 Chondrocyte isolation and fabrication of chondrocyte-laden cast hydrogels

Primary chondrocytes were harvested from macroscopically healthy full-thickness cartilage of equine metacarpophalangeal joints ($n = 3$; 3–10 years old), obtained from the local slaughterhouse. Cartilage was removed from the joints and digested overnight at 37 °C in DMEM supplemented with collagenase II (1.5 $\mu\text{g ml}^{-1}$, hyaluronidase (1 mg ml^{-1} , FBS (10%), and pen/strep (1%). After digestion, the cell suspension was filtered through a 40 μm cell strainer and the chondrocytes were stored in liquid nitrogen until further use.

Before use, chondrocytes (passage 0) were expanded in monolayer culture for ~14 d (seeding density of 5×10^3 cells cm^{-2} in chondrocyte expansion medium consisting of DMEM, FBS (10%) and pen/strep (1%). The chondrocytes were harvested when they reached 80%–90% confluence. Stock solutions of 30% M₁₀P₁₀ and 3% HAMA were prepared by dissolving the right amount of both polymers in PBS with Irgacure (0.05%) at 4 °C overnight. Next, the stock solutions were mixed at different ratios and diluted if necessary to obtain the five different formulations (table 1). Chondrocytes were mixed with the M₁₀P₁₀/HAMA mixtures on ice, to obtain a final concentration of $15\text{--}20 \times 10^6$ chondrocytes ml^{-1} ($n = 3$, concentration slightly varied per donor). Constructs were cast by injecting the cell-laden polymer mixtures into cylindrical Teflon molds (sample size: 6 mm in diameter, 2 mm in height). The molds were incubated for 15 min at 37 °C to allow physical hydrogel formation. Subsequently, chemical cross-linking was induced by irradiation with UV light (UV-Handleuchte lamp A, Hartenstein, Germany, wavelength: 365 nm, intensity at 3 cm: 1.2 mW cm^{-2} , irradiation time: 5 min). Cross-linked constructs were removed from the molds and were cultured for 28 d at 37 °C and 5% CO₂ in chondrogenic differentiation medium consisting of high glucose DMEM supplemented with ITS+ premix (1%), dexamethasone (0.1 μM), L-ascorbic acid-2-phosphate (0.2 mM), recombinant human TGF- β 1 (10 ng ml^{-1}), and pen/strep (1%) to stimulate chondrogenesis and redifferentiation of the chondrocytes [44, 45]. As a positive control, fibrin samples containing chondrocytes from the same donors were prepared and cultured as previously described [16].

2.5 Histology, immunohistochemistry, and biochemical assays

To evaluate cartilage-like tissue formation, hydrogels were harvested at days 1 and 28. Part of each sample was fixed overnight in formalin (37%) and dehydrated through a graded ethanol series. After a clearing step in xylene, the samples were embedded in paraffin. Sections with a thickness of 5 μm were generated and stained with safranin-O to visualize proteoglycans, fast green to visualize collagens, and hematoxylin to stain cell nuclei, as previously described [46]. Collagen types I, II, and VI were visualized on sections with immunohistochemistry as previously described [16]. For proteoglycan IV immunohistochemistry, the same protocol was used as previously described for collagen type VI, but with only a pronase antigen retrieval. All sections were visualized with a light microscope (Olympus BX51 microscope, Olympus DP70 camera, Hamburg, Germany). The remaining parts of the different harvested cell-laden hydrogels were weighed, freeze dried,

and weighed again to determine the water content. Next, the samples were digested overnight at 60 °C in digestion buffer (0.2 M NaH₂PO₄ + 0.01 M EDTA · 2 H₂O in milliQ, pH = 6.0) supplemented with papain (31 units mg⁻¹ protein, final concentration of 0.24 mg protein ml⁻¹) and cysteine (0.01 M). After digestion, the GAG content was determined as a measure for proteoglycan, with a dimethylmethylene blue (DMMB) assay [47], using chondroitin sulfate C as standard. The amount of DNA as a measure of proliferation was measured with the Quant-iT Pico-Green dsDNA kit and read on a spectrofluorometer (Biorad, Hercules, California, USA), according to the manufacturer's protocols. The GAG content measured at day 28 was corrected for the initial readout at day 0, due to the presence of HAMA (figure S1). This corrected GAG content was normalized to the DNA content for comparison between groups. In addition, the average change in water content normalized to the samples wet weight (wwt) was determined for each hydrogel formulation. The DNA content was normalized to the dry weight (dwt) of the samples.

2.6 Evaluation of mechanical properties of hydrogel constructs

Cell free, cylindrical hydrogels cast as described in section 2.4. were analyzed using a dynamic mechanical analyzer (DMA) (DMA Q800, TA Instruments, Etten-Leur, The Netherlands) in an uniaxial unconfined compression test, after the equilibrium state of swelling (5 h) was reached in PBS. A preload force of 0.001 N and a ramp force of 0.1 N min⁻¹ with an upper force limit of 1 N were applied, and the elastic modulus (E, Young's modulus) was calculated as the slope of the initial linear segment of the stress/strain curves ($n = 3$).

2.7 Fabrication and characterization of printed constructs with and without reinforcement

Constructs of different designs and with or without PCL reinforcement were printed with formulation M or MHA_{0.5} (table 2) using a 3DDiscovery bioprinter (regenHU, Villaz-St-Pierre, Switzerland) equipped with a Bluepoint 4 UV lamp (point light source, wavelength range: 300–600 nm, UV-A intensity at 5 cm = 103 mW cm⁻², Hönle UV Technology AG, Gräfelfing, Germany). Pneumatically driven robotic dispensers were used for the extrusion of the hydrogel and PCL filaments. The hydrogel precursor mixture was loaded into a syringe connected to a micro valve (CF300H) nozzle, while PCL pellets were loaded into a stainless steel cartridge furnished with a phosphor bronze thin-wall conical nozzle (inner diameter = 0.56 mm; Integrated Dispensing Solutions, Agoura Hills, CA). Each layer of the PCL/hydrogel hybrid constructs was generated by printing parallel filaments of PCL (strand distance = 1.5 or 2.0 mm), followed by deposition of hydrogel filaments between adjacent PCL strands. Subsequent layers were printed with a filament orientation perpendicular to that of the underlying layer. To achieve a solid or a porous hydrogel filling of the PCL framework, the hydrogel was deposited in the center of adjacent PCL filaments or at a distance of ¼ of the strand distance, respectively. Additionally, the amount of the extruded hydrogel was adjusted by varying the valve opening time (v.o.t.) and pressure (detailed print settings reported in table 3). Different temperatures of the deposition plate were used to obtain desired flowbehavior of the hydrogel after extrusion. For all designs (table 2), square sheets (15 × 15 mm) were printed with a height of 2.4 mm, and after each hydrogel layer was printed, chemical cross-linking was induced by 3 s of irradiation with the Bluepoint UV lamp from a distance of 5 cm. After printing, constructs were irradiated for an additional

time period to reach a total irradiation time of 69 s. After cross-linking, cylindrical samples were punched out of the printed sheets with a 6 mm biopsy punch, and visually inspected and photographed using an Olympus ZS61 microscope (Tokyo, Japan) coupled with an Olympus digital camera (Tokyo, Japan). As controls, hydrogelfree PCL constructs and PCL constructs infused with hydrogel by injection molding were generated. More specifically, two PCL sheets with different strand distances, i.e. 1.5 or 2.0 mm were printed as described above but without dispensing hydrogel between the PCL filaments. Subsequently, six cylindrical samples were punched out from each sheet, and three constructs per sheet were inserted in a Teflon-based injection mold, infused with the hydrogel, incubated at 37 °C for 5 min, and cross-linked for 69 s using the Bluepoint UV lamp from a distance of 5 cm. The remaining three constructs per sheet were used as hydrogel-free controls. Finally, the mechanical stiffness of the different printed constructs was evaluated using a DMA with an unconfined compression set up. Samples were preloaded with a force of 0.1 N and further compressed up to 18 N using a force ramp rate of 1.8 N min⁻¹. Young's moduli were calculated using stress strain curves.

2.8 Statistics

Statistical analysis was performed with SPSS software (version 21, IMB Corp.). For quantitative measurements of matrix production within one cell donor, a one-way analysis of variance (ANOVA) was performed, while a randomized block design ANOVA was performed for the average matrix production, to correct for donor variations. Differences in Young's moduli and viability were determined with a one-way ANOVA. Differences in Young's moduli between constructs fabricated with a different strand distance within each co-print condition were determined with an independent t-test. A significance level of 0.05 was used. When the ANOVA highlighted significant differences, a Bonferroni post hoc test was performed except for the GAG/DNA data in the cast hydrogels which were compared with a Dunnett post hoc test to explore whether the presence of HAMA had an effect compared to HAMA free hydrogels.

3 Results and discussion

3.1 Effect of HAMA concentration on chondrogenesis by embedded chondrocytes

The evaluated hydrogel formulations supported cartilage matrix production of embedded chondrocytes with a hydrogel composition-dependent extent (figure 1). During culture, rounded cell clusters rich in newly formed matrix were observed in samples with average HAMA concentrations (MHA_{0.25}, MHA_{0.5}, table 1) and to a lesser extent in the hydrogels without HAMA or with the lowest HAMA concentration (M and MHA_{0.1}). The largest cell clusters surrounded by newly formed matrix were observed in samples with the highest HAMA concentration (MHA₁), however these clusters were observed sporadically and had irregular shapes compared to the rounded clusters in the other formulations. Additionally, the cells and cell nuclei within these irregular shaped clusters had a stretched appearance (samples MHA₁). Contrarily, cells and cell nuclei in the hydrogels with lower HAMA concentrations or without HAMA contained a rounded shape after 28 d of culture. The tissue matrix around the circular cell clusters reacted strongly with the collagen type II antibody, as well as with safranin-O, indicating the presence of cartilage-like tissue (figure 1). As

safranin-O also stains HAMA, a pink color was observed in all HAMA-containing hydrogels also at day 0. However, the intensity of the staining was higher near the cells for samples at day 28. More collagen type II positive and intense red (safranin-O) areas were observed in hydrogels with intermediate HAMA concentrations (MHA_{0.25}, MHA_{0.5}) compared to hydrogels without HAMA or with the lowest HAMA concentrations (M and MHA_{0.1}). Hydrogels with formulation MHA₁ contained hardly any safranin-O positive areas at day 28, but did reveal intense collagen type II positive areas. However, the collagen type II staining was restricted to the sporadic cell clusters. On the other hand, in hydrogels with intermediate HAMA concentrations (MHA_{0.25}, MHA_{0.5}) some collagen type II positive areas were also observed in the inter-territorial regions. The presence of collagen type I, a marker for fibrocartilage, increased with increasing HAMA concentration (figure 1). Additionally, the presence of collagen type VI, a marker of chondron formation, decreased in the areas directly around the chondrocyte membranes in hydrogels with increasing HAMA concentrations, although the matrix clusters in MHA₁ stained overall positive for collagen type VI. Finally, proteoglycan IV, a zonal marker found predominantly in the cartilage surface, was mainly expressed at the hydrogel border of constructs without HAMA or with a low HAMA concentration (0.1%). Overall, all samples showed some proteoglycan IV positive areas.

Quantitative measurements for GAG content normalized to the DNA content of donor 1 and 2 (figures 2(a) and (b)) matched the visualization of GAGs with the safranin-O staining in figure 1. Contrary, no clear differences between hydrogels with different HAMA concentrations were observed in samples cultured with chondrocytes from donor 3 (figure 2(c)). This illustrates that the influence of HAMA on matrix synthesis by the chondrocytes is varying between chondrocyte donors [48, 49]. On average, significantly more GAG/DNA was measured in hydrogels with intermediate HAMA concentrations (MHA_{0.25}, MHA_{0.5}), compared to the hydrogels without HAMA (M) (figure 2(d)). Hydrogels with the lowest (MHA_{0.1}) and highest (MHA₁) HAMA concentrations did not show significant differences in GAG/DNA compared to hydrogels without HAMA (M). Samples with 1% HAMA, cultured with chondrocytes of donor 2, did contain significantly less GAG/DNA compared to the HAMA free hydrogels (figure 2(b)). Moreover, GAG/DNA levels measured in samples with intermediate HAMA concentrations (0.25%–0.5%) were similar to the fibrin controls for donors 1 and 2, while the GAG/DNA levels were higher in the fibrin samples for donor 3 (figure S2).

These observations demonstrate a dose-dependent effect of HAMA on the cartilage matrix production by chondrocytes in pHPMA-lac-PEG/HAMA hydrogels. More specifically, hydrogels with intermediate HAMA concentrations (0.25% and 0.5%) showed increased cartilage-like matrix production by the embedded cells compared to HAMA-free hydrogels, while a higher HAMA concentration (1%) stimulated a shift from hyaline cartilage to fibrocartilage formation. Chondrocytes are known to interact with HA via their membrane receptors e.g. CD44, intercellular adhesion molecule-1, and receptor for hyaluronan mediated motility [26, 50–53]. This interaction is believed to be responsible for the anabolic effect that HA can have on the matrix production by chondrocytes, as disruption of this HA-chondrocyte binding is associated with matrix degradation in native cartilage [54]. The dose-dependent response of chondrocytes to HA may be attributed to a negative feedback system,

in which limited receptor binding with HA, especially via CD44, stimulates matrix production by chondrocytes, while more receptor interactions inhibit chondrocyte redifferentiation [26, 43, 44, 55]. The hypothesis of receptor binding, would also explain why the optimal HA and HAMA concentration for cartilage matrix stimulation appears to increase with increasing cell numbers. In the present study, we demonstrate an optimum with 0.25%–0.5% HAMA in pHPMA-lac-PEG triblock copolymers based hydrogels with 20×10^6 chondrocytes ml^{-1} . Kawasaki *et al* [28] reported an optimum with 0.001%–0.01% of HA in collagen-based hydrogels with 2×10^6 chondrocytes ml^{-1} , Akmal *et al* [26] found an optimum with 0.01%–0.1% HA in alginate beads with 5×10^6 chondrocytes ml^{-1} , whereas Levett *et al* [27] found an optimum with 0.5% HAMA in collagen type I based hydrogels with 10×10^6 chondrocytes ml^{-1} . Nevertheless, in contrast to our findings, Levett *et al* [27] and Akmal *et al* [26] reported a decrease in collagen type I gene expression and protein level, respectively, by chondrocytes in hydrogels with increasing HA or HAMA concentrations. Both studies were conducted with hydrogels based on natural polymers with known cell attachment sites that influence cell behavior, which could explain the different findings [43]. Intuitively, the optimal HA or HAMA concentration for matrix production is likely also dependent on the hydrogel system in which the cells are cultured. The polymer network influences cell migration, which can affect the establishment of a receptor-HA interaction [56]. Additionally, other materials properties, such as construct stiffness and cross-linking densities, have also been demonstrated to influence cell behavior and could, therefore, also influence the response of chondrocytes to the presence of HAMA [57, 58].

The water content normalized to the samples wwt increased for all hydrogel formulations during culture with approximately 5%–7% (figure 2(e)). However, no significant differences in swelling were observed between the various formulations, regardless the HAMA content. This finding is in line with previous studies that also reported a negligible change in swelling of samples with 0%–1% HAMA [21, 27].

The DNA content normalized to the samples' dwt significantly increased for all hydrogel formulations during the culture period (figure 2(c)). All hydrogel formulations reached a similar DNA/dwt content at day 28 ($\sim 50\text{--}70 \mu\text{g mg}^{-1}$), implying that all hydrogels supported proliferation to a similar extent. Although HA is capable to influence proliferation of multiple cell types, this was not observed in the current study for chondrocytes, in line with Levett *et al* [27]. Contrarily, Kawasaki *et al* [28], Akmal *et al* [26], and Park *et al* [23], reported an increase in DNA content due to the presence of HA. However, the initial cell densities used in those studies were lower compared to the cell density used by Levett *et al* [27] and by us in the current study which may explain the observed difference [59]. Additionally, Akmal *et al* [26] only observed an increase in proliferation in hydrogels with the lowest HA concentrations, suggesting that this effect can also be dose-dependent and thus not present in the higher HA concentrations used by Levett *et al* [27] and in this study.

3.2 Effect of HAMA concentration on hydrogel mechanical properties

All studied hydrogel formulations were shape-stable after swelling in PBS (5 h). Young's moduli ranged from 14.0 ± 0.6 to 30.8 ± 0.9 kPa (figure 3).

Figure 3 shows that the Young's modulus of $M_{10}P_{10}$ /HAMA hydrogels increased with increasing HAMA concentration. The Young's moduli of all evaluated hydrogel formulations were statistically different from each other, except for MHA0.1 and MHA0.25 that had similar moduli. Clearly, the presence of HAMA led to stiffer hydrogels compared to hydrogel M, despite an equal total polymer concentration, i.e. 20% w/w and a comparable total number of methacrylate groups. These findings are in line with our previous observations [15] and can find an explanation in the microstructure of these hydrogels. $M_{10}P_{10}$ /HAMA hydrogels are known to exhibit phase separation [60], as also observed in the safranin-O histology at day 0 (figure 1) for HAMA-containing hydrogels. We have recently demonstrated that micro-phase separation in these hydrogels leads to the formation of highly hydrated, HAMA-rich domains and partially dehydrated more hydrophobic regions, where the majority of $M_{10}P_{10}$ is located [60]. The extent of this phase separation is highly dependent on the HAMA concentration. In that study, we have also found that when using low HAMA concentrations (<1% w/w), the relative increase in $M_{10}P_{10}$ concentration in the hydrophobic domains due to their partial dehydration (driven by the presence of HAMA), resulted in stiffer physical hydrogels. In a similar way, this phenomenon could explain the effect of HAMA concentration on the Young's moduli of chemically cross-linked hydrogels found in the present study. The effect of HAMA on construct stiffness may also be partially attributed to the much higher MW of HAMA (120 kDa) compared to that of $M_{10}P_{10}$ (40 kDa). In fact, the relatively longer HAMA molecules are likely able to generate more chain entanglements that provide higher stiffness to the entire polymer network. The general increase of hydrogel stiffness with increasing HAMA concentration, likely responsible for a tighter network in hydrogels with higher HAMA content, can also explain the observed cell clusters with irregular shapes and confined matrix deposition in the histological analysis of MHA₁ hydrogels. In fact, it has been reported that dense polymer networks can hamper the diffusion of newly formed matrix [11, 29, 61]. In addition, the differences in construct stiffness may also contribute to the difference in matrix production by the embedded chondrocytes [57, 58].

3.3 Fabrication of hydrogel/PCL co-printed constructs

Among all evaluated hydrogel formulations, hydrogels containing 0.5% HAMA (MHA_{0.5}) induced the highest cartilage-like tissue formation, and displayed a medium/high Young's modulus, which is beneficial for the hydrogel filament stability during printing and handling. Hence, the printing experiments were performed with this formulation. Additionally, the incorporation of 0.5% HAMA introduced yield stress behavior to MHA_{0.5} (yield stress = 28.7 ± 0.2 Pa), which is reported to improve shape-fidelity of 3D bioprinted constructs [11, 16, 62, 63], whereas in accordance with our previously reported findings [17], no yield stress was found for the HAMA-free formulation M (control, figure S3). In fact, 3D printing of shape-stable MHA_{0.5} constructs without supporting structures or reinforcement was successfully achieved (figure 4(a)). Printing of PCL under optimized conditions and using a strand distance of 1.5 or 2.0 mm, resulted in the generation of stiff thermoplastic meshes with interconnected pores (figure 4(f)). For the coprinting of PCL and MHA_{0.5}, constructs with four different designs, having a PCL framework with variable strand distance and a final architecture with or without pores, were printed (Figures 4(b)-(e) and (g)-(j)). To obtain porosity in pMH/PCL constructs, a hydrogel dispensing pressure of 0.1 MPa and a v.o.t. of

300 μ s were used. To obtain solid co-printed constructs, higher v.o.t. (500 or 1300 μ s when using a strand distance of 1.5 and 2.0 mm, respectively) and a slightly higher pressure (0.13 MPa, when using a strand distance of 2.0 mm) were used to increase the amount of extruded hydrogel. The temperature of the deposition plate was set at 35 °C while printing solid constructs. In contrast, a higher temperature, i.e. 40 °C was found to be beneficial for the stability of the hydrogel filaments, required to maintain a constant shape and size of the pores in the porous co-printed constructs (pMH/PCL_2 and pMH/PCL_4).

Figure 4(k) shows that PCL meshes without hydrogel and with a strand distance of 1.5 and 2.0 mm possessed Young's moduli of 7.3 ± 0.4 and 5.1 ± 0.7 MPa, respectively. The Young's moduli of pMH/PCL co-printed constructs ranged from 3.5 and 4.6 MPa, with slightly higher values for constructs with lower strand distance (i.e. 1.5 mm), and no statistical difference between porous and non-porous constructs. Porosity is considered beneficial for cartilage tissue engineering as it facilitates the nutrients/waste products exchange between the cell-laden hydrogel matrix and the surrounding fluids [64, 65]. Moreover, pore size and organization have been shown to affect *in vivo* tissue maturation of tissue engineered constructs [66, 67]. Additionally, in an *in vivo* orthotopic scenario, cell-free co-printed porous scaffolds combined with marrow-stimulation techniques e.g. microfracture, may facilitate penetration of stem cells from the bone marrow into the implanted hydrogels [68].

Importantly, all the PCL-based constructs had Young's moduli of approximately three orders of magnitude higher than non-reinforced hydrogel constructs (figure 3), reaching a stiffness comparable to that of native cartilage (0.4–0.8 MPa) [69–71]. This result confirmed the suitability of PCL as reinforcing material for cartilage tissue engineering, in line with previously reported findings [72, 73]. Interestingly, co-printed PCL/hydrogel constructs had lower Young's moduli compared to the hydrogel-free PCL meshes. This finding was reproducible and the decrease was significant for constructs with a strand distance of 1.5 mm. In contrast, printed PCL meshes infused with hydrogel MHA_{0.5} had similar Young's moduli as the hydrogel-free PCL meshes (7.9 ± 0.3 and 6.4 ± 0.9 MPa for constructs with strand distance of 1.5 and 2.0 mm, respectively), indicating that the difference in construct stiffness is a result of the coprinting process. Likely, the layer-by-layer hydrogel deposition partially interfered with the adhesion of newly printed PCL filaments with underlining PCL strands. Nevertheless, co-printed constructs were macroscopically stable and the PCL skeleton appeared intact and coherent to the desired design, after selective removal of the hydrogel for visualization purposes (data not shown). However, this observation highlights the critical role of the chosen print settings and construct design on the mechanical properties of the final construct.

4 Conclusions

In this study, hydrogel-based cartilage repair constructs with optimized bioactivity and mechanical properties were successfully fabricated, via the addition of HAMA to a thermosensitive pHPMA-lac-PEG hydrogel and via co-printing with PCL. Results of the HAMA concentrations screening demonstrate a dose-dependent effect of HAMA on the cartilage matrix production by embedded chondrocytes. More specifically, intermediate

HAMA concentrations (0.25%–0.5%) increased cartilage-like matrix production compared to HAMA-free hydrogels, while higher (1%) concentrations resulted in undesirable fibrocartilage formation. These results may impact the choice of HAMA content in bio-ink development. In addition, the presence of HAMA was found to increase the construct stiffness with increasing concentration. These findings allowed the identification of an optimal hydrogel composition of 19.5% pHPMA-lac-PEG with 0.5% HAMA. This formulation supported increased cartilage matrix production compared to HAMA-free hydrogels, contained limited fibrocartilage formation, and displayed a medium/high Young's modulus, and yielding behavior, beneficial for the 3D printing of these hydrogels. Hydrogel/PCL co-printing enabled the generation of complex 3D constructs with mechanical stiffness in the range of native cartilage. However, the co-printing procedure influenced the final construct properties, highlighting the crucial role of the print settings in determining the final construct properties. In conclusion, we developed advanced composite cartilage repair constructs, with a chondrogenic hydrogel component and a mechanically adequate PCL reinforcement. Whilst this further mimics biomechanical properties of native articular cartilage, this is an interesting approach for further optimization.

Supplementary Material

Refer to Web version on PubMed Central for supplementary material.

Acknowledgments

The research leading to these results has received funding from the Dutch Arthritis Foundation (LLP-12), the European Community's Seventh Framework Programme (FP7/2007–2013) under grant agreement no. 309962 (HydroZONES) and the European Research Council under grant agreement no. 647426 (3D-JOINT).

The authors would like to thank Mattie H P van Rijen and Naveed A Rahman for their assistance with histology and biochemical assays, as well as Maarten M Blokzijl for his contribution to the 3D printing experiments, Anneloes Mensinga for her assistance with the cell cultures, and Carl C L Schuurmans for his contribution to the synthesis of M₁₀P₁₀ polymer. The primary antibody against collagen type II (II-II6B3) and collagen type VI (5C6), developed by T F Linsenmayer and E S Engvall, respectively, were obtained from the DSHB developed under the auspices of the NICHD and maintained by The University of Iowa, Department of Biology, Iowa City, IA 52242.

Nomenclature

3D	three-dimensional
ANOVA	analysis of variance
CP	cloud point
DM	degree of methacrylation
DMA	dynamic mechanical analyzer
DMEM	Dulbecco's modified eagle medium
DMMB	dimethylmethylene blue
dwt	dry weight
FBS	fetal bovine serum

GAG	glycosaminoglycan
HA	hyaluronic acid
HAMA	methacrylated hyaluronic acid
HPMA	<i>N</i> -(2-hydroxypropyl) methacrylamide
ICAM-1	intercellular adhesion molecule-1
LCST	lower-critical solution temperature
MW	molecular weight
PBS	phosphate buffered saline
PCL	polycaprolactone
PEG	polyethylene glycol
pen/strep	penicillin/streptomycin
pHPMA-lac	methacrylated poly[<i>N</i> -(2-hydroxypropyl)methacrylamide mono/dilactate]
s.d.	strand distance
v.o.t.	valve opening time

References

- [1]. Murphy SV, Atala A. 3D bioprinting of tissues and organs. *Nat Biotechnol.* 2014; 32:773–85. [PubMed: 25093879]
- [2]. Buckley MR, Gleghorn JP, Bonassar LJ, Cohen I. Mapping the depth dependence of shear properties in articular cartilage. *J Biomech.* 2008; 41:2430–7. [PubMed: 18619596]
- [3]. Silverberg JL, Barrett AR, Das M, Petersen PB, Bonassar LJ, Cohen I. Structure-function relations and rigidity percolation in the shear properties of articular cartilage. *Biophys J.* 2014; 107:1721–30. [PubMed: 25296326]
- [4]. Schuurman W, et al. Zonal chondrocyte subpopulations reacquire zone-specific characteristics during *in vitro* redifferentiation. *Am J Sports Med.* 2009; 37:97s–04s. [PubMed: 19846691]
- [5]. Almaraz AJ, Athanasiou KA. Design characteristics for the tissue engineering of cartilaginous tissues. *Ann Biomed Eng.* 2004; 32:2–17. [PubMed: 14964717]
- [6]. Prakash D, Learmonth D. Natural progression of osteo-chondral defect in the femoral condyle. *Knee.* 2002; 9:7–10. [PubMed: 11830374]
- [7]. Mouser VHM, et al. Three-dimensional bioprinting and its potential in the field of articular cartilage regeneration. *Cartilage.* 2016; doi: 10.1177/1947603516665445
- [8]. Klein TJ, Malda J, Sah RL, Hutmacher DW. Tissue engineering of articular cartilage with biomimetic zones. *Tissue Eng B.* 2009; 15:143–57.
- [9]. Liao J, Shi K, Ding Q, Qu Y, Luo F, Qian Z. Recent developments in scaffold-guided cartilage tissue regeneration. *J Biomed Nanotechnol.* 2014; 10:3085–104. [PubMed: 25992430]
- [10]. Malda J, et al. 25th anniversary article: engineering hydrogels for biofabrication. *Adv Mater.* 2013; 25:5011–28. [PubMed: 24038336]
- [11]. Mouser VHM, Melchels FPW, Visser J, Dhert WJA, Gawlitta D, Malda J. Yield stress determines bioprintability of hydrogels based on gelatin-methacryloyl and gellan gum for cartilage bioprinting. *Biofabrication.* 2016; 8

- [12]. Vermonden T, et al. Photopolymerized thermosensitive hydrogels: synthesis, degradation, and cytocompatibility. *Biomacromolecules*. 2008; 9:919–26. [PubMed: 18288801]
- [13]. Censi R, et al. Photopolymerized thermosensitive hydrogels for tailorable diffusion-controlled protein delivery. *J Control Release*. 2009; 140:230–6. [PubMed: 19527757]
- [14]. Censi R, et al. Photopolymerized thermosensitive poly (HPMA lactate)-PEG-based hydrogels: effect of network design on mechanical properties, degradation, and release behavior. *Biomacromolecules*. 2010; 11:2143–51. [PubMed: 20614933]
- [15]. Censi R, et al. A printable photopolymerizable thermosensitive p(HPMAm-lactate)-PEG hydrogel for tissue engineering. *Adv Funct Mater*. 2011; 21:1833–42.
- [16]. Abbadessa A, et al. A synthetic thermosensitive hydrogel for cartilage bioprinting and its biofunctionalization with polysaccharides. *Biomacromolecules*. 2016; 17:2137–47. [PubMed: 27171342]
- [17]. Abbadessa A, et al. A thermo-responsive and photopolymerizable chondroitin sulfate-based hydrogel for 3D printing applications. *Carbohydrate Polym*. 2016; 149:163–74.
- [18]. Ponta H, Sherman L, Herrlich PA. CD44: from adhesion molecules to signalling regulators. *Nat Rev Mol Cell Biol*. 2003; 4:33–45. [PubMed: 12511867]
- [19]. Lesley J. Hyaluronan binding by cell surface CD44. *J Biol Chem*. 2000; 275:26967–75. [PubMed: 10871609]
- [20]. Liao J, Qu Y, Chu B, Zhang X, Qian Z. Biodegradable CSMA/PECA/graphene porous hybrid scaffold for cartilage tissue engineering. *Sci Rep*. 2015; 5
- [21]. Levett PA, Melchels FPW, Schrobback K, Hutmacher DW, Malda J, Klein TJ. A biomimetic extracellular matrix for cartilage tissue engineering centered on photocurable gelatin, hyaluronic acid and chondroitin sulfate. *Acta Biomater*. 2014; 10:214–23. [PubMed: 24140603]
- [22]. Chung C, Erickson IE, Mauck RL, Burdick JA. Differential behavior of auricular and articular chondrocytes in hyaluronic acid hydrogels. *Tissue Eng A*. 2008; 14:1121–31.
- [23]. Park H, Choi B, Hu J, Lee M. Injectable chitosan hyaluronic acid hydrogels for cartilage tissue engineering. *Acta Biomater*. 2013; 9:4779–86. [PubMed: 22935326]
- [24]. Liao E, Yaszemski M, Krebsbach P, Hollister S. Tissue-engineered cartilage constructs using composite hyaluronic acid/collagen I hydrogels and designed poly(propylene fumarate) scaffolds. *Tissue Eng*. 2007; 13:537–50. [PubMed: 17319795]
- [25]. Allemann F, Mizuno S, Eid K, Yates KE, Zaleske D, Glowacki J. Effects of hyaluronan on engineered articular cartilage extracellular matrix gene expression in 3-dimensional collagen scaffolds. *J Biomed Mater Res*. 2001; 55:13–9. [PubMed: 11426390]
- [26]. Akmal M, et al. The effects of hyaluronic acid on articular chondrocytes. *J Bone Joint Surg*. 2005; 87-B:1143–9.
- [27]. Levett PA, Hutmacher DW, Malda J, Klein TJ. Hyaluronic acid enhances the mechanical properties of tissue-engineered cartilage constructs. *PLoS One*. 2014; 9:e113216. [PubMed: 25438040]
- [28]. Kawasaki K, Ochi M, Uchio Y, Adachi N, Matsusaki M. Hyaluronic acid enhances proliferation and chondroitin sulfate synthesis in cultured chondrocytes embedded in collagen gels. *J Cell Physiol*. 1999; 179:142–8. [PubMed: 10199553]
- [29]. Bryant SJ, Anseth KS. Hydrogel properties influence ECM production by chondrocytes photoencapsulated in poly (ethylene glycol) hydrogels. *J Biomed Mater Res*. 2002; 59:63–72. [PubMed: 11745538]
- [30]. Schuurman W, Khristov V, Pot MW, van Weeren PR, Dhert WJA, Malda J. Bioprinting of hybrid tissue constructs with tailorable mechanical properties. *Biofabrication*. 2011; 3
- [31]. Jang J, Lee J, Seol Y-J, Jeong YH, Cho D-W. Improving mechanical properties of alginate hydrogel by reinforcement with ethanol treated polycaprolactone nanofibers. *Composites B*. 2013; 45:1216–21.
- [32]. Iviglia G, Cassinelli C, Torre E, Bains F, Morra M, Vitale-Brovarone C. Novel bioceramic-reinforced hydrogel for alveolar bone regeneration. *Acta Biomater*. 2016; 44:97–109. [PubMed: 27521494]
- [33]. Lee J-S, Hong JM, Jung JW, Shim J-H, Oh J-H, Cho D-W. 3D printing of composite tissue with complex shape applied to ear regeneration. *Biofabrication*. 2014; 6

- [34]. Kundu J, Shim J-HH, Jang J, Kim S-WW, Cho D-WW. An additive manufacturing-based PCL-alginate chondrocyte bioprinted scaffold for cartilage tissue engineering. *J Tissue Eng Regen Med*. 2015; 9:1286–97. [PubMed: 23349081]
- [35]. Visser J, et al. Biofabrication of multi-material anatomically shaped tissue constructs. *Biofabrication*. 2013; 5
- [36]. Melchels FPW, et al. Hydrogel-based reinforcement of 3D bioprinted constructs. *Biofabrication*. 2016; 8
- [37]. Martin JJ, Fiore BE, Erb RM. Designing bioinspired composite reinforcement architectures via 3D magnetic printing. *Nat Commun*. 2015; 6
- [38]. Woodruff MA, Hutmacher DW. The return of a forgotten polymer—polycaprolactone in the 21st century. *Prog Polym Sci*. 2010; 35:1217–56.
- [39]. Olubamiji AD, Izadifar Z, Si JL, Cooper DML, Eames BF, Chen DX. Modulating mechanical behaviour of 3D-printed cartilage-mimetic PCL scaffolds: influence of molecular weight and pore geometry. *Biofabrication*. 2016; 8
- [40]. Woodfield TBF, Malda J, de Wijn J, Péters F, Riesle J, van Blitterswijk CA. Design of porous scaffolds for cartilage tissue engineering using a three-dimensional fiberdeposition technique. *Biomaterials*. 2004; 25:4149–61. [PubMed: 15046905]
- [41]. Neradovic D, van Steenberghe MJ, Vansteelant L, Meijer YJ, van Nostrum CF, Hennink WE. Degradation mechanism and kinetics of thermosensitive polyacrylamides containing lactic acid side chains. *Macromolecules*. 2003; 36:7491–8.
- [42]. Neradovic D, van Nostrum CF, Hennink WE. Thermoresponsive polymeric micelles with controlled instability based on hydrolytically sensitive N-isopropylacrylamide copolymers. *Macromolecules*. 2001; 34:7589–91.
- [43]. Hachet E, Van Den Berghe H, Bayma E, Block MR, Auzély-Velty R. Design of biomimetic cell-interactive substrates using hyaluronic acid hydrogels with tunable mechanical properties. *Biomacromolecules*. 2012; 13:1818–27. [PubMed: 22559074]
- [44]. Benya P. Dedifferentiated chondrocytes reexpress the differentiated collagen phenotype when cultured in agarose gels. *Cell*. 1982; 30:215–24. [PubMed: 7127471]
- [45]. Guo J, Jourdain GW, Maccallum DK. Culture and growth characteristics of chondrocytes encapsulated in alginate beads. *Connect Tissue Res*. 1989; 19:277–97. [PubMed: 2805684]
- [46]. Wall, A, Board, T. Chemical basis for the histological use of safranin O in the study of articular cartilage. *Classic Papers in Orthopaedics*. London: Springer; 2014. 433–5.
- [47]. Farndale RW, Sayers CA, Barrett AJ. A direct spectrophotometric microassay for sulfated glycosaminoglycans in cartilage cultures. *Connect Tissue Res*. 1982; 9:247–8. [PubMed: 6215207]
- [48]. Gawlitta D, van Rijen MHP, Schrijver EJM, Alblas J, Dhert WJA. Hypoxia impedes hypertrophic chondrogenesis of human multipotent stromal cells. *Tissue Eng A*. 2012; 18:1957–66.
- [49]. Zwickl H, Niculescu-Morzsa E, Nehrer S. Investigation of collagen transplants seeded with human autologous chondrocytes at the time of transplantation. *Cartilage*. 2010; 1:194–9. [PubMed: 26069551]
- [50]. Yasuda T. Nuclear factor- κ B activation by type II collagen peptide in articular chondrocytes: its inhibition by hyaluronan via the receptors. *Mod Rheumatol*. 2012; 23:1116–23. [PubMed: 23224053]
- [51]. Viola M, et al. Biology and biotechnology of hyaluronan. *Glycoconj J*. 2015; 32:93–103. [PubMed: 25971701]
- [52]. Dowthwaite GP, Edwards JCW, Pitsillides AA. An essential role for the interaction between hyaluronan and hyaluronan binding proteins during joint development. *J Histochem Cytochem*. 1998; 46:641–51. [PubMed: 9562572]
- [53]. Onodera Y, Teramura T, Takehara T, Fukuda K. Hyaluronic acid regulates a key redox control factor Nrf2 via phosphorylation of Akt in bovine articular chondrocytes. *FEBS Open Bio*. 2015; 5:476–84.
- [54]. Ariyoshi W, Takahashi N, Hida D, Knudson CB, Knudson W. Mechanisms involved in enhancement of the expression and function of aggrecanases by hyaluronan oligosaccharides. *Arthritis Rheumatol*. 2012; 64:187–97.

- [55]. Schuh E, Hofmann S, Stok K, Notbohm H, Müller R, Rotter N. Chondrocyte redifferentiation in 3D: the effect of adhesion site density and substrate elasticity. *J Biomed Mater Res A*. 2012; 100:38–47. [PubMed: 21972220]
- [56]. Vu LT, Jain G, Veres BD, Rajagopalan P. Cell migration on planar and three-dimensional matrices: a hydrogel-based perspective. *Tissue Eng B*. 2015; 21:67–74.
- [57]. Discher DE. Tissue cells feel and respond to the stiffness of their substrate. *Science*. 2005; 310:1139–43. [PubMed: 16293750]
- [58]. Huang G, et al. Engineering three-dimensional cell mechanical microenvironment with hydrogels. *Biofabrication*. 2012; 4
- [59]. Heng BC, et al. Effect of cell-seeding density on the proliferation and gene expression profile of human umbilical vein endothelial cells within *ex vivo* culture. *Cytherapy*. 2011; 13:606–17. [PubMed: 21171823]
- [60]. Unpublished data.
- [61]. Kock LM, Geraedts J, Ito K, van Donkelaar CC. Low agarose concentration and TGF- β 3 distribute extracellular matrix in tissue-engineered cartilage. *Tissue Eng A*. 2013; 19:1621–31.
- [62]. Jungst T, Smolan W, Schacht K, Scheibel T, Groll J. Strategies and molecular design criteria for 3D printable hydrogels. *Chem Rev*. 2016; 116:1496–539. [PubMed: 26492834]
- [63]. Melchels FPW, Dhert WJA, Hutmacher DW, Malda J. Development and characterisation of a new bioink for additive tissue manufacturing. *J Mater Chem B*. 2014; 2:2282–9. [PubMed: 32261716]
- [64]. Hollister SJ. Porous scaffold design for tissue engineering. *Nat Mater*. 2006; 5:590–590.
- [65]. Hutmacher DW. Scaffolds in tissue engineering bone and cartilage. *Biomaterials*. 2000; 21:2529–43. [PubMed: 11071603]
- [66]. Malda J, et al. The effect of PEGT/PBT scaffold architecture on oxygen gradients in tissue engineered cartilaginous constructs. *Biomaterials*. 2004; 25:5773–80. [PubMed: 15147823]
- [67]. Malda J, et al. The effect of PEGT/PBT scaffold architecture on the composition of tissue engineered cartilage. *Biomaterials*. 2005; 26:63–72. [PubMed: 15193881]
- [68]. Steadman JR, Rodkey WG, Rodrigo JJ. Microfracture: surgical technique and rehabilitation to treat chondral defects. *Clin Orthop Relat Res*. 2001; 391:S362–9.
- [69]. Chen AC, Bae WC, Schinagl RM, Sah RL. Depth-and strain-dependent mechanical and electromechanical properties of full-thickness bovine articular cartilage in confined compression. *J Biomech*. 2001; 34:1–12. [PubMed: 11425068]
- [70]. Athanasiou KA, Agarwal A, Dzida FJ. Comparative study of the intrinsic mechanical properties of the human acetabular and femoral head cartilage. *J Orthop Res*. 1994; 12:340–9. [PubMed: 8207587]
- [71]. Jurvelin JS, Buschmann MD, Hunziker EB. Optical and mechanical determination of Poisson's ratio of adult bovine humeral articular cartilage. *J Biomech*. 1997; 30:235–41. [PubMed: 9119822]
- [72]. Visser J, et al. Reinforcement of hydrogels using three-dimensionally printed microfibres. *Nat Commun*. 2015; 6
- [73]. Boere KWM, et al. Biofabrication of reinforced 3D-scaffolds using two-component hydrogels. *J Mater Chem B*. 2015; 3:9067–78. [PubMed: 32263038]

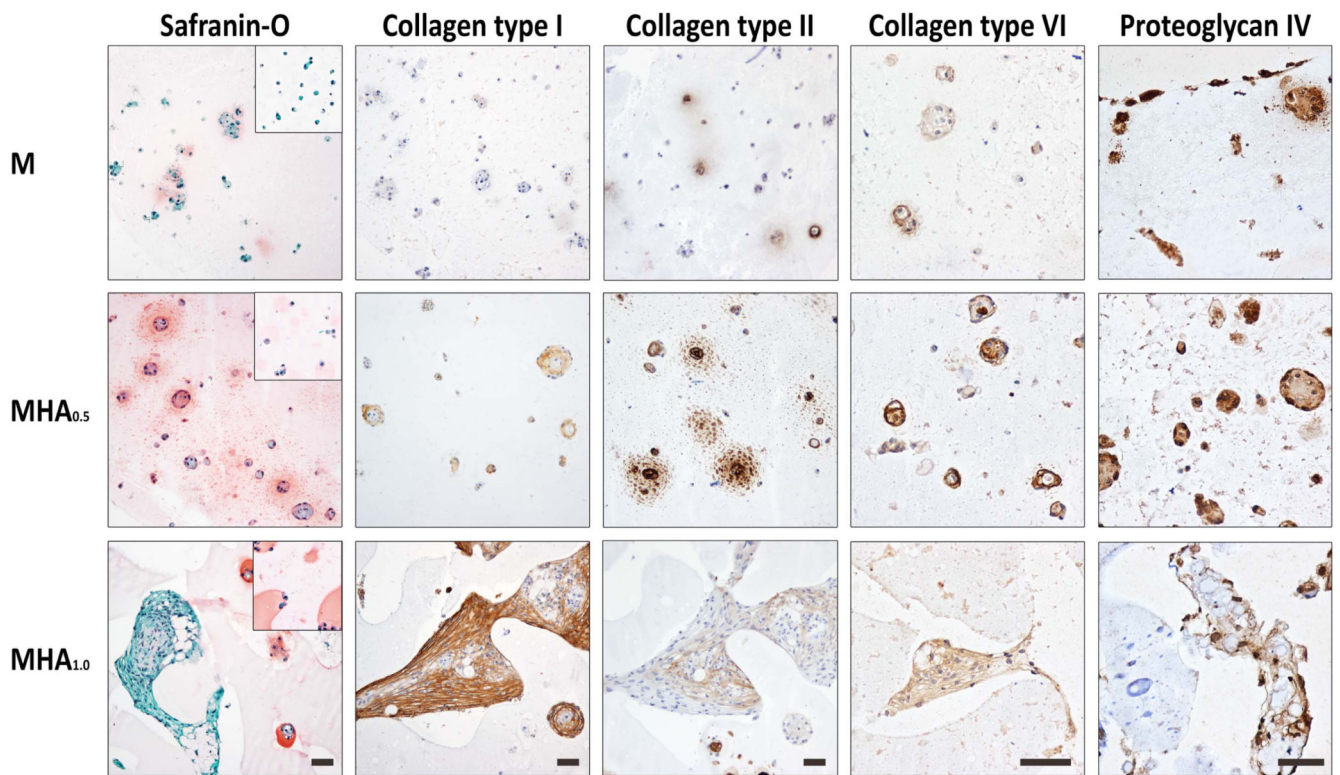


Figure 1.

Overview of the histology and immunohistochemistry of chondrocytes cultured in M₁₀P₁₀/HAMA hydrogels with different HAMA concentrations for 28 d. Scale bar represent 50 μ m and it is the same for all images of the same staining. Square insert in the safranin-O images are from day 1 samples.

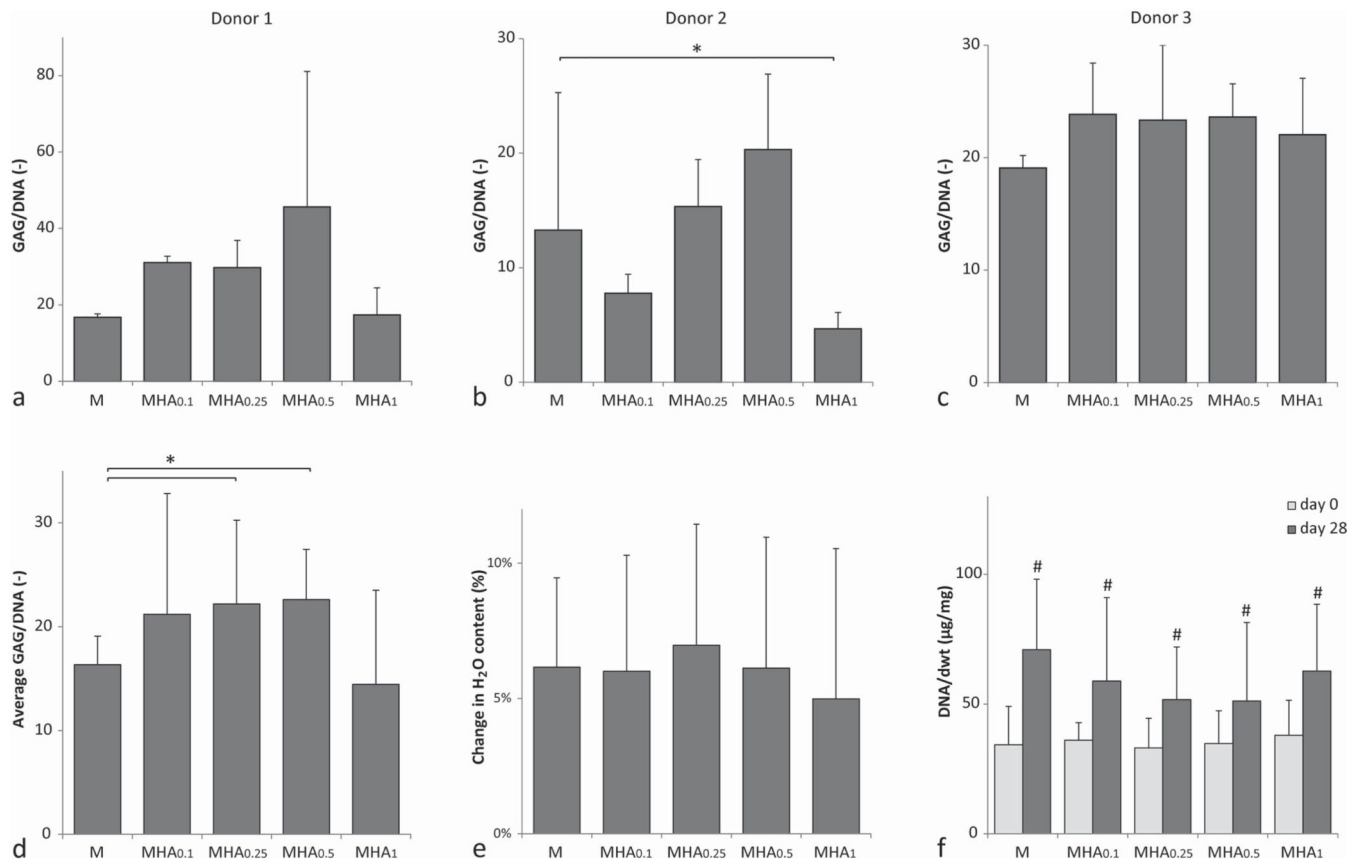


Figure 2.

Biochemical analysis of multiple chondrocyte-laden hydrogel formulations. (a)–(d) GAG content normalized to the DNA content at day 28 for (a) donor 1, (b) donor 2, (c) donor 3, and (d) the average of all donors. (e) Difference in water content between day 28 and day 0. (f) DNA content normalized to the dwt. * indicates a significant difference between the groups. # indicates a significant difference compared to groups without a # but similar to groups with a #.

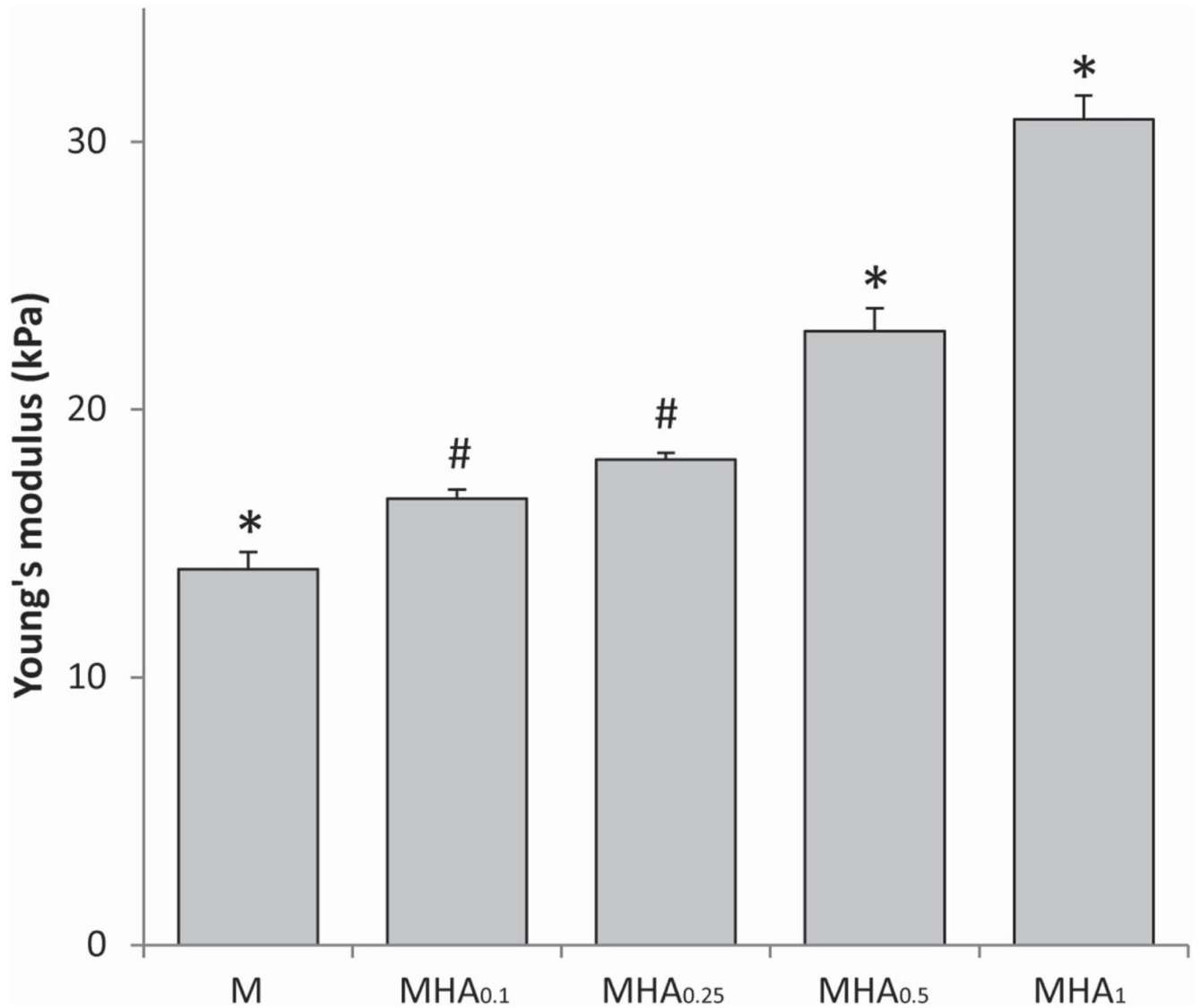


Figure 3.

Young's moduli obtained from stress/strain curves which were generated with unconfined compression, where * indicates a significant difference ($p < 0.05$) from all other groups and # indicates a significant difference to all groups except to each other.

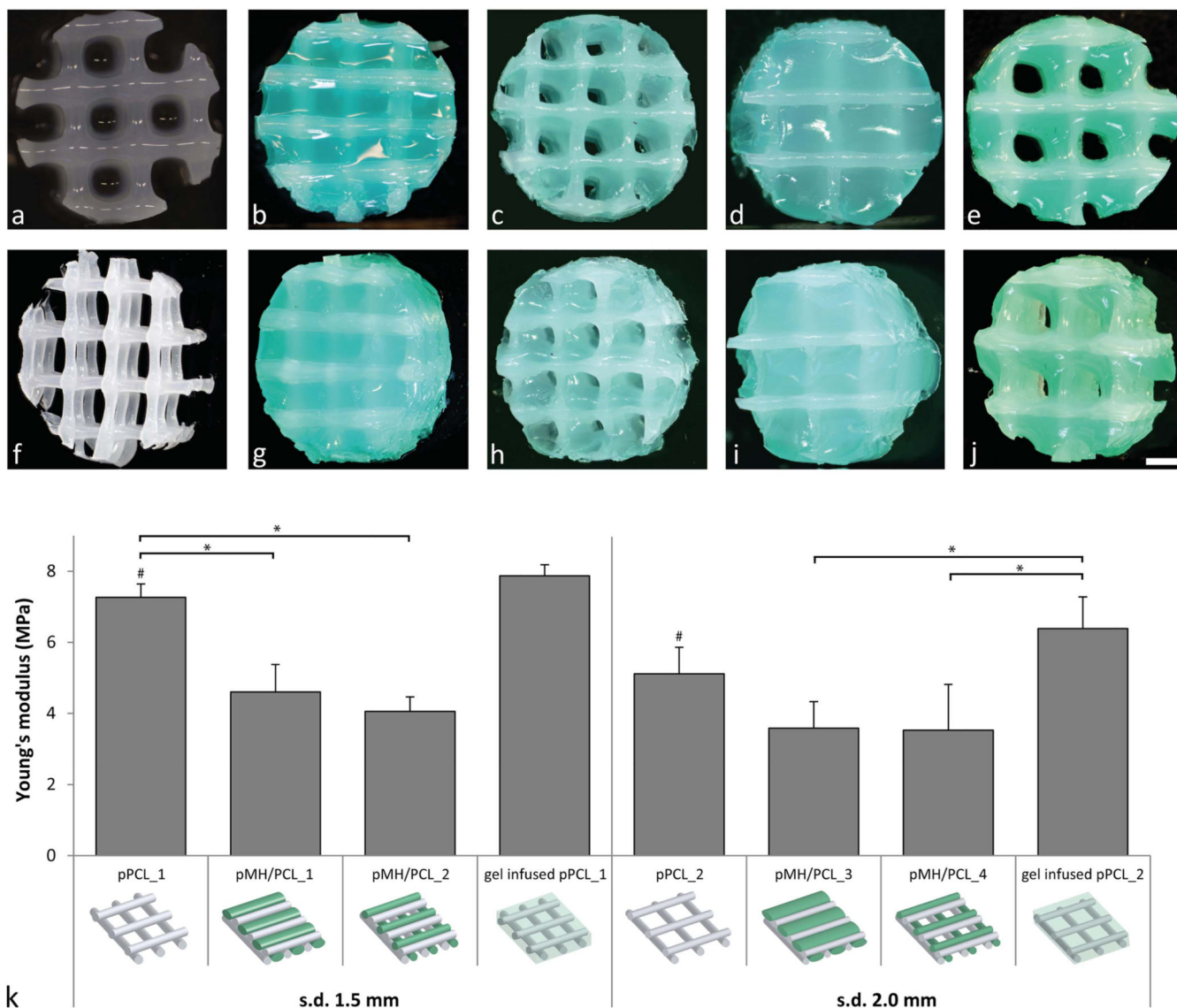


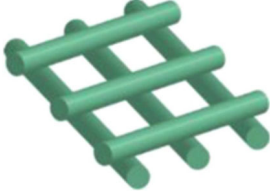
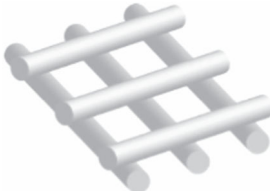
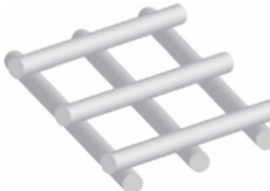
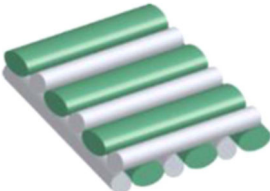
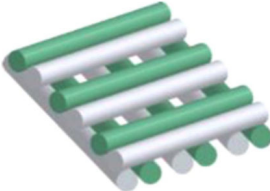
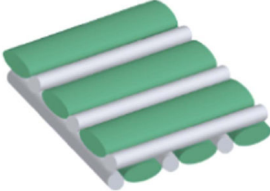
Figure 4.

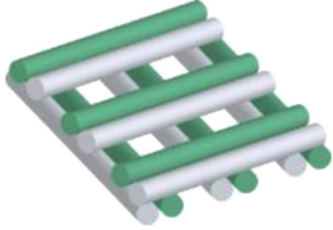
Evaluation of co-printed constructs. (a) Top view of a 3D shape stable printed hydrogel construct with formulation $MHA_{0.5}$. (b) and (g) Top and top-side view of pMH/PCL_1 ($MHA_{0.5}$ /PCL, non-porous, strand distance = 1.5 mm). (c) and (h) Top and topside view of pMH/PCL_2 ($MHA_{0.5}$ /PCL, porous, strand distance = 1.5 mm). (d) and (i) Top and top-side view of pMH/PCL_3 ($MHA_{0.5}$ /PCL, non-porous, strand distance = 2.0 mm). (e) and (j) Top and top-side view of pMH/PCL_4 ($MHA_{0.5}$ /PCL, porous, strand distance = 2.0 mm). (f) Top-side view of a PCL reinforcement structure. (k) Young's moduli of the different printed constructs. Significant differences ($p < 0.05$) between conditions with the same strand distance are indicated with *, while # indicates a significant difference between strand distance within the same print conditions. For visualization purposes, $MHA_{0.5}$ hydrogel was stained green in the reinforced constructs. Scale bar represent 1 mm and it is the same for all images, s.d. = strand distance.

Table 1
Overview of the concentrations of M₁₀P₁₀ and HAMA in PBS for the five evaluated hydrogel formulations with their abbreviations.

Abbreviation	Polymer concentration(% w/w)	
	M ₁₀ P ₁₀	HAMA
M	20	—
MHA _{0,1}	19.9	0.1
MHA _{0,25}	19.75	0.25
MHA _{0,5}	19.5	0.5
MHA ₁	19	1

Table 2
Construct designs for printing with hydrogel MHA_{0.5} (green) with and without PCL (white) reinforcement.

Abbreviation	Materials	Layer design	Description ^a
pMH	MHA _{0.5}		Porous s.d. = 1.5 mm
pPCL_1	PCL		Porous s.d. = 1.5 mm
pPCL_2	PCL		Porous s.d. = 2.0 mm
pMH/PCL_1	MHA _{0.5} + PCL		Solid s.d. = 1.5 mm
pMH/PCL_2	MHA _{0.5} + PCL		Porous s.d. = 1.5 mm
pMH/PCL_3	MHA _{0.5} + PCL		Solid s.d. = 2.0 mm

Abbreviation	Materials	Layer design	Description ^a
pMH/PCL_4	MHA _{0,5} + PCL		Porous s.d. = 2.0 mm

^a s.d. = strand distance.

Table 3
Optimized settings applied for the 3D printing of hydrogel, PCL and hydrogel/PCL constructs.

pMH	Hydrogel print settings	PCL print settings
Pressure	0.1 MPa	
Temperature		
Cartridge	37 °C	
Deposition plate	40 °C	
XY plane speed	40 mm s ⁻¹	—
Microvalve CF300H		
Dosing distance	0.1 mm	
Valve opening time	300 μs	
PCL	Hydrogel print settings	PCL print settings
Pressure		0.3 MPa
Temperature		
Cartridge		80 °C
Deposition plate	—	35 °C
<i>XY plane speed</i>		1 mm s ⁻¹
pMH/PCL	Hydrogel print settings	PCL print settings
Pressure	0.1 ^a or 0.13 ^b MPa	0.3 MPa
Temperature		
Cartridge	37 °C	80 °C
Deposition plate	35 ^c or 40 ^d °C	35 ^c or 40 ^d °C
XY plane speed	40 mm s ⁻¹	1 mm s ⁻¹
Microvalve CF300H		
Dosing distance	0.1 mm	
Valve opening time	300 ^e , 500 ^f or 1300 ^g μs	

^a Applied to pMH_1, pMH_2 and pMH_4.

^b Applied to pMH_3.

^c Applied to pMH_1 and pMH_3.

^d Applied to pMH_2 and pMH_4.

^e Applied to pMH_2 and pMH_4.

^f Applied to pMH_1.

^g Applied to pMH_3.